Quantum and Classical Calculations of Ground State Properties of Parabolic Quantum Dots.

V. Popsueva,[1,2] T. Matthey,[3] J. P. Hansen,[1] L. Kocbach,[1] and M. Hjorth-Jensen[4,5]

[1]*Department of Physics and Technology, University of Bergen, N-5007 Bergen, Norway*
[2]*Center of Mathematics for Applications, University of Oslo, N-0316 Oslo, Norway*
[3]*Bergen Center for Computational Science, N-5008 Bergen, Norway*
[4]*Department of Physics and Center of Mathematics for Applications, University of Oslo, N-0316 Oslo, Norway*
[5]*Department of Physics and Astronomy, Michigan State University, East Lansing, Michigan 48824, USA*

We report calculations for electronic ground states of parabolically confined quantum dots for up to 30 electrons based on the quantum Monte Carlo method. Effects of the electron-electron interaction and the response to a magnetic field are exposed. The wavefunctions and the ground state energies are compared with purely classical calculations performed with a comprehensive Molecular Dynamics code. For the chosen well parameters a close correspondence in the overall shape of electron density distribution is found even for small number of electrons, while the detailed radial distributions show the effects of Pauli principle in the quantal case.

I. INTRODUCTION

The experimental and technological advances in production and use of two-dimensional quantum dot structures provide also new challenges and possibilities for theoretical studies reaching into surprisingly wide areas of physics [1]. For example, techniques for monitoring of controlled single-electron coherent transport through double dot systems has recently been realized [2]. Studies of structural properties of few- [3, 4] and many-electron systems [5–8] are in this perspective of crucial importance for experimental progress. In particular coherent and quasi-coherent dynamics of quantum dots with a large number of electrons pose both theoretical and experimental challenges. 'Large' is here used in the sense 'larger than two', but still too few to justify application of mean field approaches [9]. Coherent dynamics and the interaction with a classical environment leading to decoherence are so far a highly unexplored area of the border between quantum and classical physics.

Shell-filling effects in quantum dots were demonstrated as oscillations in the addition energy spectra with increasing number of electrons in the dot almost ten years ago [10]. A few years earlier the ground state energies as function of an external magnetic field were measured [11]. These findings sparked off an intense activity on the applications of well-known quantum mechanical structure theories from atomic and nuclear physics to the new area of quantum dots. The Hartree-Fock (HF) method, Linear Combinations of Atomic Orbitals (LCAO) methods, Density Functional Theory (DFT) and the quantum Monte-Carlo (QMC) methods are here the most frequently applied (cf. e.g. [13]) working tools which have been used and further developed in quantum dot studies. In structure theory it is well known that LCAO combined with excact diagonalization rapidly becomes computationally impractical with increasing number of electrons. HF, DFT and QMC theories are in general much more applicable with increasing particle size. The DFT method method has successfully reproduced experimental addition energy spectra [12], while similar success of the HF method has not yet

been reported. The HF method as well as mean field models do however give rise to oscillatory addition energy spectra [14] as well. Various QMC approaches have investigated the role of correlations, confinement geometry and shell effects for zero external magnetic field, see eg. [15–19]. The onset of a magnetic field introduces an additional parameter in the Hamiltonian and thus an implicit dependence of the N-electron energy levels as function of the field. It is well known that with increasing (weak) field the various field free energy levels depend differently on the field which leads to an intricate spectrum of (avoided) level crossings. It was for example recently shown that the character of ground state of a two-electron double dot changes from a $S = 0$ type to a $S = 1$ and back to $S = 0$ type as the field strength is increased [3]. The behavior of many-particle systems in magnetic fields has previously been investigated for up to 13 electrons [6, 8] by QMC methods.

In this paper we apply a new QMC procedure [20] to study the ground state properties of parabolically confined two-dimensional quantum dots. We calculate addition energy spectra for dots with 2 to 20 electrons and we display the behavior of the ground state for increasing magnetic field. Further more, the energy and the probability density are compared with purely classical electron dynamics calculations. These are based on the employment of non-equilibrium molecular dynamics methods where a thermostat slowly cools the system to a near-frozen state.

In the following section we briefly describe the theoretical models and the computational methods. The results are displayed and discussed in section III followed by concluding remarks in section IV.

II. MODELS

Our model Hamiltonian $\hat{H}$ of N identical electrons parabolically confined in two dimensions $r_i = (x_i, y_i)$ is

given by

$$\hat{H} = \sum_{i=1}^{N} \left[-\frac{\hbar^2}{2m^*}\nabla_i^2 + V(\mathbf{r}_i) + \sum_{j<i}^{N} \frac{e^2}{4\pi\epsilon\epsilon_0|\mathbf{r}_i - \mathbf{r}_j + \alpha|} \right].$$
(1)

Here m^* is the effective electron mass and ϵ is the dielectric constant of the background material. Realistic experimental values for a two dimensional structure surrounded by a GaAs material is $m^* = 0.067m_e$ where m_e is the electron mass and $\epsilon = 13.5$. The parameter α is empirically introduced to mimic a finite confinement size in the $\hat{z}-$ direction. A non-zero α will generally increase the mean distance between real confined dot electrons and thereby reduce the role of electron-electron interactions. The confining harmonic potential is defined by the frequency ω_0 which in real systems typically is $\hbar\omega_0 \sim 2 - 6$ meV.

In addition the dot electrons may be exposed to a constant magnetic field, $\mathbf{B}$, in the $\hat{z}-$direction which correspond to an electromagnetic vector potential $\mathbf{A} = \frac{1}{2}B(-\mathbf{e}_x + -\mathbf{e}_y)$. The effective external single particle potential can then be brought to the form,

$$V(\mathbf{r}_i) = \frac{1}{2}m^*\omega^2 r_i^2 + \frac{w_B}{2}\hat{L}_z,$$
(2)

with $\hat{L}_z$ being the angular momentum operator of the $\hat{z}-$ axis. The effective confining potential is given by $w^2 = \omega_0^2 + \frac{\omega_B^2}{4}$, where $\omega_B = \frac{|eB|}{2m^*}$ is the Larmor frequency. In the following we apply reduced atomic units and set $\omega = \hbar = m^* = 1$.

A. Variational Monte Carlo

In the contruction of the single-particle basis and the trial wave function to be used in our variational Monte Carlo simulations we follow closely the work of Harju *et al.*, see for example Ref. [6, 7].

We thus assume that the electrons in the quantum dot move in a two-dimensional parabolic potential, meaning in turn that the one-body problem is similar to the classical harmonic oscillator problem. In scaled units, our ansatz for the single-particle basis is given by

$$\psi_{n,\pm|m|} \propto (x \pm iy)^{|m|}L_{(n-|m|/2)}^{|m|}(r^2)\exp{-(\frac{r^2}{2})},$$
(3)

with n being the shell index, m the angular momentum and $r^2 = x^2 + y^2$. Since this is also a system with no well-defined center of mass motion, we need, in order to obtain a translationally invariant Hamiltonian to redefine the coordinates through

$$x \pm iy = (x - x_{\text{cm}}) \pm \imath(y - y_{\text{cm}}),$$
(4)

where x_{cm} and y_{cm} are the center of mass coordinates. In addition to the harmonic oscillator part for the single-particle motion we assume as discussed above that the electrons interact via repulsive Coulomb forces.

Our ansatz for the many-body wave function consists thus of a Slater determinant multiplied by a two-body correlation function $f(r_{ij})$, leading to the following form for the N-particle trial wave function Ψ_N

$$\Psi_N = \det[\psi_1\psi_2\ldots\psi_N] \times \prod_{i<j}^{N} f(r_{ij}),$$
(5)

where ψ_i refer to the single-particle wave functions defined in Eq. (3) with the index i representing the single-particle state i with quantum numbers n, m and positions $(x_i - x_{\text{cm}}) \pm \imath(y_i - y_{\text{cm}})$. The single-particle wave functions depend on x and y and the center of mass coordinates x_{cm} and y_{cm}. In our approach here we do not introduce variational parameters in the single-particle wave functions of Eq. (3), see also the discussions in Refs. [6].

For the two-body correlation function we assume one of the simplest possible Jastrow factors, namely

$$f(r_{ij}) = \exp{\left(\frac{a_1 r_{ij}}{1 + a_2 r_{ij}}\right)},$$
(6)

with a_1 and a_2 being variational parameters. Note that these parameters are different for fermion pairs with parallel and anti-parallel spins, respectively. This leads in total to four variational parameters in our calculations. Note also that the correlation function does not depend on the center of mass motion. The work of Alexander and Coldwell [26] contains an extensive list of correlation functions for light atoms systems.

The norm of the total wave function is not needed since it is redundant in the Metropolis sampling. For more details on the Metropolis sampling and variational and diffusion Monte Carlo techniques see for example Refs. [6, 7, 27, 28]. We apply here a standard Metropolis sampling, as discussed in for example Refs. [6, 7] where the main problem is to integrate

$$E[\Psi_N] = \frac{\int \Psi_N^* \hat{H} \Psi_N d\mathbf{x}}{\int \Psi_N^* \Psi_N d\mathbf{x}}.$$
(7)

In our discussion below, we compare the energies obtained with the above correlated wave function with those arising from the non-interacting case, given by the sum over single-particle energies determined by the harmonic oscillator function. These energies are given by the Fock-Darwin energy spectrum [29]

$$\epsilon_{mn} = \hbar\omega(n_x + n_y + |m| + 1) - \frac{1}{2}\hbar\omega m.$$
(8)

All simulations in this work were performed with 10^7 Monte Carlo cycles (and 5×10^5 thermalisation steps). There are two variational parameters in the Jastrow factor of Eq. (6), $a_1 = 1.0$ and $a_2 = 1.5$ are found to give consistently optimized results for all considered values of N. In Table II we show some of the simulation results for different values of N, with a_1 and β as described above.

We also compare our classical results with those obtained by V. M. Bedanov and F. Peeters. The energies in the table are given in units of meV. In addition, we observe a few differences in electron configurations. Following configurations are different in [30]: 10:(2,8) 11:(3,8), 19:(1,6,12).

N	Electron configuration	total energy	total energy [a]
1	1	0	0
2	2	2.507	10.671
3	3	5.263	13.101
4	4	8.656	16.511
5	5	12.611	20.861
6	1,5	17.094	26.000
7	1,6	22.201	31.844
8	1,7	27.881	38.523
9	2,7	34.026	45.963
10	3,7	40.629	54.021
11	4,7	47.786	62.686
12	3,9	55.337	72.039
13	4,9	63.417	81.984
14	4,10	71.940	92.597
15	5,10	80.914	103.791
16	1,5,10	90.287	115.571
17	1,6,10	100.059	127.882
18	1,6,11	110.321	140.715
19	1,7,11	120.954	154.179
20	1,7,12	132.073	168.171

[a]V. M. Bedanov and F. Peeters,[30]

TABLE I: Selected simulation results, energy and standard deviation for different electron configurations and various N-values.

N	Electron configuration	energy	standard deviation
2	↑↓	3.15853	0.000408482
2	↑↑	3.61921	7.99765e-05
3	↑↓↑	6.65201	0.000489449
6	$3 \times (↑↓)$	21.4633	0.000900802
12	$6 \times (↑↓)$	68.7905	0.000904738
20	$10 \times (↑↓)$	169.413	0.00284978

TABLE II: Selected simulation results, energy and standard deviation for different electron configurations and various N-values.

B. Classical calculations

A classical mechanics-based "molecular dynamics" approach is well suited for massive particles at sufficient high temperatures, for example in simulations of molecular liquids. Several classical simulations of low temperature and confined dilute matter systems have also been successfully applied recently, see for example Ref. [21]. We apply the same program in the present work except that the $\hat{z}$-direction is kept frozen.

In essence, the dynamics is described by Newton's equation of motion through

$$m_i \frac{d^2}{dt^2}\mathbf{r}_i(t) = \mathbf{F}_i(t),$$ (9)

where the Force $\mathbf{F}$ is derived from Eq. (1) and modified at each time step Δt according to,

$$\mathbf{F_i} \leftarrow \mathbf{F_i} - \zeta \mathbf{v_i} \frac{1}{\mathbf{N\Delta t}}.$$ (10)

The thermostat ζ slowly drives the system from a non-equilibrium initial configuration to the final state characterized by a required temperature T',

$$\frac{d\zeta}{dt} = \gamma(E_k(t) - \frac{3N}{2}kT').$$ (11)

Here E_k is the kinetic energy, k is Boltzmann's constant and γ is a parameter of order unity which plays no role for the final structures, but regulates the computational speed of cooling/heating of the system. The temperature T' is the set equilibrium temperature of the system.

When propagating the system in time we solve Eq. (9) numerically with an appropriate time step by the leap-frog method [22]. Time steps and cooling parameters are carefully adjusted to avoid the system to be locked into any local energy minima close to the absolute minimum as described in [23].

III. RESULTS AND DISCUSSION

A. Energy levels

In Fig. 1 we show the resulting ground state energies as functions of the number of electrons N and with zero magnetic field and confinement energy $\hbar\omega_0 = 3$ meV. The two upper curves are the variational Monte Carlo energies obtained without and with the Jastrow factor described in the previous section. This factor is seen to play an increasing role for increasing number of electrons, as expected since the average distance between the electrons decreases with increasing electrons in the dot. For $N = 20$ electrons the Jastrow factors decreases the energy with about 10%. To compare with the total role of the electron-electron interaction we also plot in Fig. 1 the corresponding ground state for non-interacting particles, full line with circles. The role of the correlations is again seen to increase with the number of electrons, but much less than for the interacting case. Finally, in the same figure we display the ground state energy obtained with the classical molecular dynamics calculations. As expected the energies are a factor of two below the quantal interacting energies due to vanishing kinetic energy for $T = 0$.

In Fig. 2 we show that both the quantum and the classical energy scales as power law in N, i.e. we can write $E(N) \sim const \cdot N^n$. In the quantum mechanical case, this function can be written as $E(N) = E(1)N^{1.81}$, and for the classical case as $E(N) = E(1)N^{1.58}$. We expect the power exponent n to be between 1 and 2. The Coulomb repulsion energy term that is proportional to N^2 is reduced because of screening, so we get a value somewhat lower. We also observe that this term is more important in the quantum mechanical case than in the classical case.
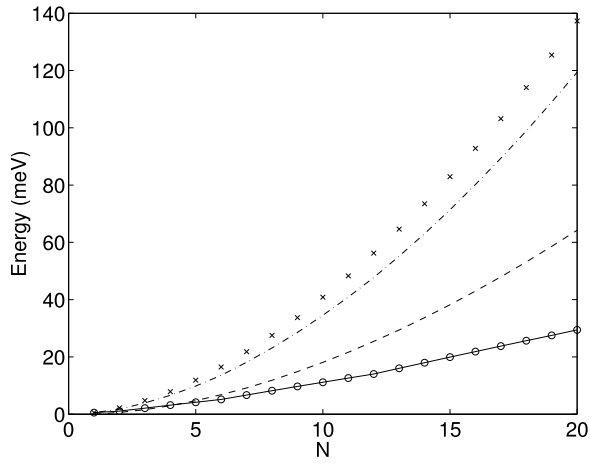
FIG. 1: Ground state energy as a function of number of electrons ($\alpha = 0, B = 0$). Crosses: QMC calculation without Jastrow factor; dashed-dotted line: QMC with the Jastrow factor. Full line with circles: Independent particle energies. Dashed line: Classical calculation.
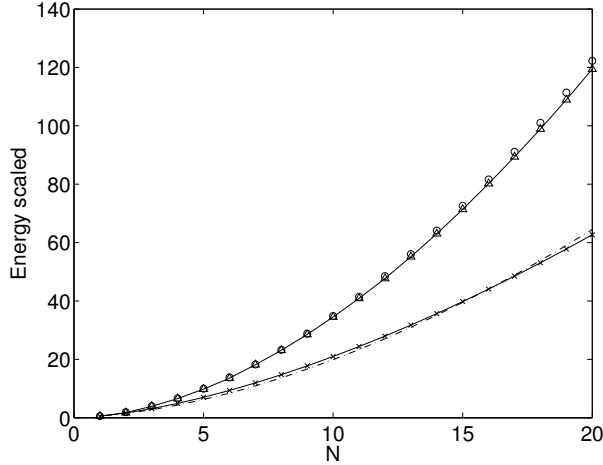

FIG. 2: Ground state energy as a function of number of electrons ($B = 0$). Triangles: QMC calculation; circles: total ground state energy scaled as function of N. Dashed-dotted line: classical calculation; crosses: classical energy, scaled as a function og N.

All calculations in Fig. **??** are performed with $\alpha = 0$, see Eq. (1). In Fig. **??** the role of screening is examined by computing the addition energy spectra with $\hbar\omega_0 = 3$ meV. The addition spectra is given by, $\delta\mu = E(N+1) - 2E(N) + E(N-1)$, where μ is the chemical potential. The energies have been evaluated with $\alpha = 0, 5$ and 10 nm. Strong peaks at $N = 2$ and $N = 6$ and higher "magic" numbers are obtained in all cases, in qualitative agreement with experiment. The strong peak for $N = 4$ gets reduced for increasing α and the calculations for $\alpha = 10$nm are in better agreement with experiment than the $\alpha = 0$ case. One can argue for a finite α value since a quantum dot has a finite thickness, resulting in a screened
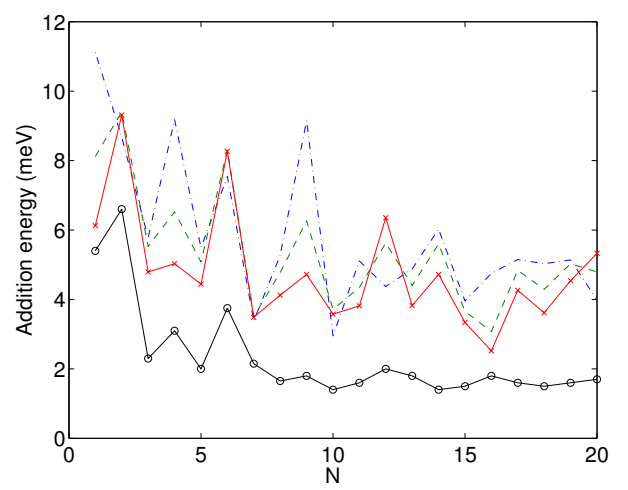

FIG. 3: (Color online) Addition energy spectrum, computed for the $\hbar\omega_0 = 3$meV-case, with different offsets α. The blue line corresponds to $\alpha = 0$ nm. Points on the green line are computed with $\alpha = 5$ nm, and those marked with x's are with $\alpha = 10$ nm. The points on the black line are those obtained from the experiment of Ref. [10].

Coulomb interaction between the electrons. This leads to a reduction in the total energy and makes the harmonic oscillator potential more dominant. We also notice that the addition energy is large at the half-filled shells $N = 4, 9, 12...$ According to Hund's rule, these are the states with maximum total spin, i.e. the electron eigenspins are parallel. Such configurations require an antisymmetric spatial wave function, which minimises the Coulomb repulsion between the electrons by keeping electrons apart and making the configuration more stable. By screeening the electrons we reduce the effect of the Coulomb repulsion, therefore also making the spatial antisymmetrisation less important for lowering the energy of the configuration. Therefore, the addition energy peaks at half-filled shells become smaller as we increase the screening parameter α.

We now turn to the non-zero magnetic field configurations. The detailed lifting of the ground state energies with magnetic fields is of great importance for coherent transport in coupled double dots. The tunneling amplitude between dots depends exponentially on the barrier parameters and energy levels which again can be adiabatically tuned by a time dependent external field. In Fig. 4 the total energy of a two- and one-particle ground state as a function of magnetic field strength is shown, in the two-electron case with and without the electron-electron interaction. As expected, with zero total orbital momentum, the energy increases monotonous with the magnetic field. The contribution from the Coulomb repulsion is seen to be very significant already for two electrons as it accounts for around 40% of the total energy.

The importance of the Coulomb repulsion increases with increasing magnetic field. Introducing a finite offset α puts a limit on how close the electrons may approach each other. This will of course prevent the Coulomb interaction from
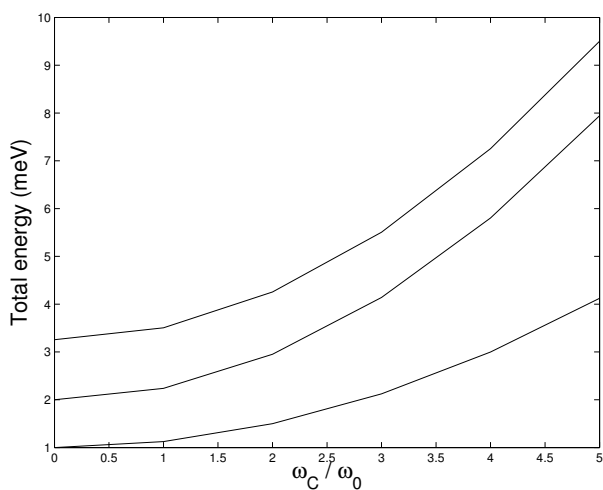
FIG. 4: Total energy of a two-particle ground state as a function of the strength of the magnetic field. Upper curve: Two particles with the electron-electron interaction. Middle curve: Two particles with no electron-electron interaction. Lower curve: A single electron. The screening parameter is $\alpha = 10$.
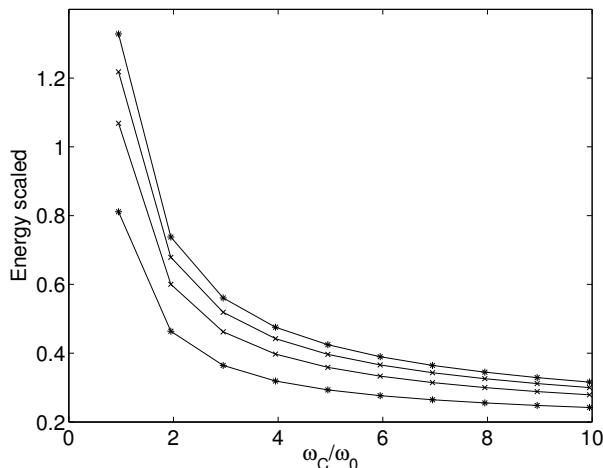

FIG. 5: Total energy per particle as a function of magnetic field strength for $N = 6, 12$ and 20, scaled by the factor $\frac{\omega_C}{\omega}$.

growing with magnetic field when the offset α is large enough. In Fig. 5 we plot the scaled total energy as a function of magnetic field strength for $N = 6$, $N = 12$ and $N = 20$ electrons. In this figure we plot the scaled total energy as a function of $\frac{\omega_C}{\omega_0}$. As the magnetic field increases, the total energy becomes close to a linear function of $\frac{\omega_C}{\omega_0}$. The energies show very similar behaviour, which can be explained by the fact that they all correspond to closed shell configurations.

## B. Electron probability distribution

We now turn to a detailed comparison of the quantal ground state probability distribution in absence of a magnetic field with corresponding classical calculations. In Fig. 6 the classical electron configurations (left) with the single-electron probability density obtained after integration over the remaining $N - 1$ electron's, $\rho(r_N) = \int dr_1...dr_{N-1}|\Psi_N|^2$ (right) are shown. The classical frozen state is taken directly from the final positions and placed on top of a figure with each electron position rotating a number of uniformly distributed angles with constant radius.

For the classical results of Fig. 6, the black dots represent electron positions obtained from freezing an initial distribution to $T' = 0$. By keeping $T' > 0$, but small, we also produce a classical spatial density distribution by time averaged superpositions of a large number of instantaneous configurations as described in Ref. [25]. These densities are represented by shades of gray superimposed over the static electron positions. The $N = 6$ configuration is identical to the one obtained in Ref. [23]. It contains a single electron in the middle and five electrons in an outer ring. This double structure is also seen for $N = 12$, but now with 3 electrons in the inner ring. The $N = 19$ configuration not shown here but published in [23] contains the first triple ring with one electron in the center, six electrons in the middle ring and 12 in the outer ring. It is interesting to note that when adding one extra electron, the $N = 20$ configuration minimizes energy by placing the extra electron in the middle ring.

Comparison between classical and quantal probability density distributions shows as expected a clear discrepancy for $N = 2$ since anti symmetrization results in a spatial symmetric wave function with a large probability of finding an electron in the trap center. For $N = 6$ the quantal ground state is a single ring with no inner electron, again due to antisymmetry, while the classical $N = 6$ configuration has a centrally positioned electron. This pattern remains valid also for the remaining two cases, viz., where the classical calculations yield a centrally placed electron, the quantal calculations show a central density dip at the center, while the absence of central electron in the classical configuration ($N = 2$ and $N = 12$) is matched by increased central density in the quantal case. In the quantal displays the gray shade coding has been selected to visualize the density variations which are of the order of about $10 - 30\%$ in the $N = 12$ and $N = 20$ cases. Apart from this effect of the Pauli principle the systematics of the main shells for $N = 6$, $N = 12$ and $N = 20$ compare well in spatial distribution with the corresponding classical ones, showing that the classical static configurations may roughly describe the ranges of the charge density distributions even for systems with relatively few confined electrons.

The grayscale in quantum densities is such that it reflects the density variations which are increasingly smaller and smaller with the number of electrons in the inner region (about 40 percent in the N=6 case, about 20 for n=20 and around 10 percent for the largest N-values. These variations reflect the nodal structure of the last filled oscillator shell. The top or dip in the central region follows the parity of the last filled
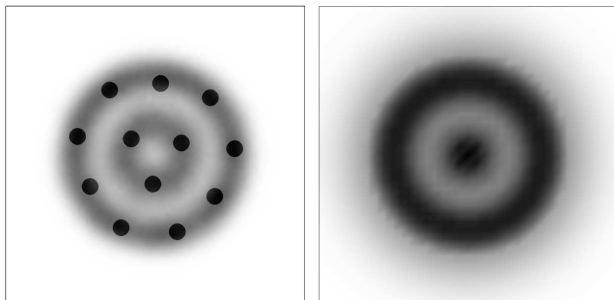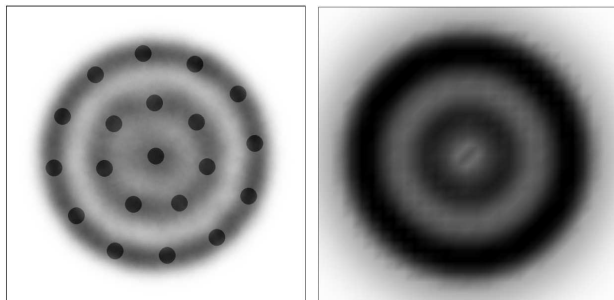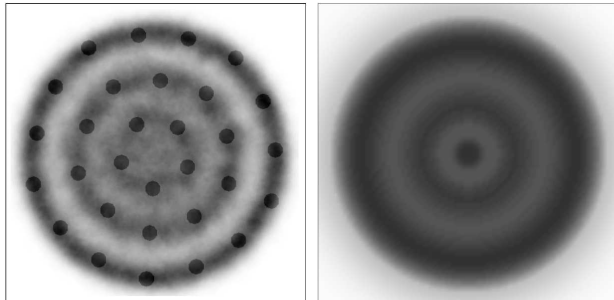
$N = 2$:
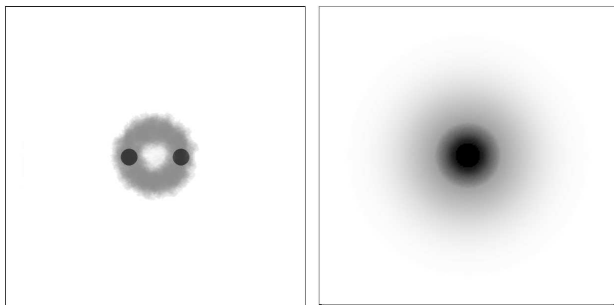
$N = 6$:
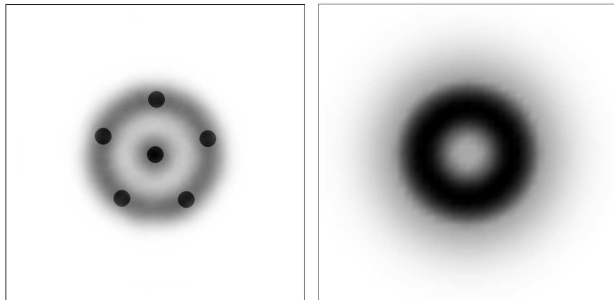
$N = 12$:

$N = 20$:

$N = 30$:

FIG. 6: Classical electron configuration (left) and quantum mechanical electron density (right) for closed shell ground states for N=2,6,12 20 and 30 electrons. The scale of all figures are from -300 nm to 300 nm in both directions.

shell which is negative for N=6,20 and positive for N=12,30. For N=30 there are 3 visible quantal and classical shells, the inner "inversion" is again obvious. Half of the classical electrons occupy the outer shell somewhat smaller than the quantal probability density for the reason discussed above. We close by concluding that even if there are distinct quantum features exposed in the right panels, the shell structure and the sizes of the classical systems show a surprisingly good correspondence with the quantal structures.

IV. CONCLUSION

The present investigation has demonstrated the usefulness of the Quantum Monte Carlo method for studies of relatively large numbers electrons inside a quantum dot with parameters typically achieved in experiments. Studies of the effects of the magnetic field have shown that the energy per particle increase due to the magnetic field is amplified by the electron repulsion, roughly proportional to the number of electrons. his follows from comparisons with the non-interacting cases and can be traced to the fact that the repulsion leads to increased expectation values of the charge distribution radius and the fact that the energetic effects of the magnetic field depends on this quantity.

The quantal calculations were compared with classical Molecular Dynamics calculations of the static equilibrium positions of classical charges confined by a harmonic force. The comparisons for closed shells shows that for the chosen type of quantum dots, the effect of the Pauli principle leads to differing behavior of the classical configurations and the quantal distributions in the central area. The overall shell structure in the quantal and classical case nevertheless has a remarkable agreement in shape and spatial extension. This points further to the possibility that a range of important dynamical processes in quantum dots may be understood from purely classical models.

[1] S. M. Reimann and M. Manninen, Rev. Mod. Phys. **74**, 1283 (2002).

[2] T. Hayashi, T. Fujisawa, H. D. Cheong, Y. H. Jeong, and Y. Hirayama, Phys. Rev. Lett. **91**, 226804 (2003).

[3] A. Harju, S. Siljamäki, and R. M. Nieminen, Phys. Rev. Lett. **88**, 226804 (2002).

[4] J. R. Petta, A. C. Johnson, C. M. Marcus, M. P. Hanson, and A. C. Gossard, Phys. Rev. Lett. **93**, 186802 (2004).

[5] E. H. Lieb, J. P. Solovej, and J. Yngvason, Phys. Rev. B **51**, 10646 (1995).

[6] A. Harju, V. A. Sverdlov, R. M. Nieminen, and V. Halonen, Phys. Rev. B **59**, 5622 (1999).

[7] A. Harju, preprint arXiv:cond-mat/0505053, unpublished.

[8] A. D. Güçlü, Jian-Sheng Wang, and Hong Guo, Phys. Rev. B **68**, 035304 (2003).

[9] E. Lipparini, *Modern Many-Particle Physics: Atomic Gases, Quantum Dots And Quantum Fluids*, (World Scientific, Singapore, 2003).

[10] S. Tarucha, D. G. Austing, T. Honda, R. J. van der Hage, and L. P. Kouwenhoven, Phys. Rev. Lett. **77**, 3613 (1996).

[11] R. C. Ashoori, H. L. Stormer, J. S. Weiner, L. N. Pfeiffer, K. W. Baldwin, and K. W. West, Phys. Rev. Lett. **71**, 613 (1993).

[12] S. M. Reimann, M. Koskinen and M. Manninen, Phys. Rev. B **59**, 1613 (1999).

[13] E. Merzbacher, *Quantum Mechanics* (Wiley, New York, 1998).

[14] M. Rontani, F. Rossi, F. Manghi, and E. Molinari, Phys. Rev. B **59**, 10165 (1999).

[15] J. Harting, O. Mülken, and P. Borrmann, Phys. Rev. B **62**, 10207 (2000).

[16] P. Sundqvist, S. Yu. Volkov, Yu. E. Lozovik, and M. Willander, Phys. Rev. B **66**, 075335 (2002).

[17] F. Pederiva, C. J. Umrigar, and E. Lipparini, Phys. Rev. B **62**, 8120 (2000).

[18] E. Räsänen, H. Saarikoski, V. N. Stavrou, A. Harju, M. J. Puska, and R. M. Nieminen, Phys. Rev. B **67**, 235307 (2003).

[19] I.-H. Lee, Y.-H. Kim, and K.-H. Ahn, J. Phys. C **13**, 1987 (2001).

[20] V. Popsueva, Master of Science thesis, *Quantum Dots - A Monte Carlo Simulation*, University of Oslo (2004), unpublished.

[21] T. Matthey, J. P. Hansen and M. Drewsen, Phys. Rev. Lett. **91**, 165001 (2003).

[22] T. Matthey, *Framework Design, Parallelization and Force Computation in Molecular Dynamics*, PhD thesis, University of Bergen (2002).

[23] F. Bolton and U. Rössler, Superlattices Microstruct. **13**, 139 (1993).

[24] B. L. Hammond, W. A. Webster Jr., and P. J. Reynolds, *Monte Carlo Methods in ab initio Quantum Chemistry* (World Scientific, Singapore, 1994).

[25] J. P. Hansen, J. Lu, L. B. Madsen, H. M. Nilsen, Phys. Rev. A **64**, 033418 (2001).

[26] S. A. Alexander and R. L. Coldwell, Int. J. Quantum Chem. **63**, 1001 (1997).

[27] F. Bolton, Phys. Rev. B **54**, 4780 (1996)

[28] B. S. Pudliner, V. R. Pandharipande, J. Carlson, S. C. Pieper, R. B. Wiringa, Phys. Rev. C **56**, 1720 (1997).

[29] V. Fock, Z. Phys. **47**, 446 (1928); C. G. Darwin, Proc. Cambridge Philos. Soc. **27**, 87 (1930).

[30] V. M. Bedanov and F. M. Peeters, Phys. Rev. B **49**, 2667 (1994).